

A cost-energy based methodology for small-scale linear Fresnel reflectors on flat roofs of urban buildings

C. Bayón-Cueli ^c, A. Barbón ^a, L. Bayón ^{b,*}, N. Barbón ^a

^a Department of Electrical Engineering, University of Oviedo, Campus of Gijón, Spain

^b Department of Mathematics, University of Oviedo, Campus of Gijón, Spain

^c Polytechnic School of Engineering of Gijón, University of Oviedo, Spain



ARTICLE INFO

Article history:

Received 20 February 2019

Received in revised form

12 June 2019

Accepted 1 July 2019

Available online 4 July 2019

Keywords:

Linear Fresnel reflector

Urban buildings

Optimization

ABSTRACT

This paper proposes a new methodology for determining the geometrical parameters and the optimal distribution of small-scale linear Fresnel reflectors on flat roofs of urban buildings. This engineering problem is highly complex as it involves 21 variables; in contrast to present-day studies available in the literature, our method provides a global solution. The algorithm involves several stages, in which it uses multiple objective functionals: maximization of the used area of the roof, minimization of the cost, minimization of losses. The solution found by this method combines all the relevant aspects from the technical and/or economic point of views and obtains, as the final objective, the maximization of the absorbed annual energy for the stated problem.

© 2019 Elsevier Ltd. All rights reserved.

1. Introduction

Without a doubt, environmental pollution has become one of the world's major concerns due to the considerable increase in greenhouse gas emissions over the past years. This worldwide concern has led to Member States of the European Union (EU) signing the Kyoto Protocol [1]. This commitment to the Kyoto Protocol entails binding obligations and the promulgation of European directives in this respect. The protocol has been renewed, extending the commitment period to 2013–2020 [2]. The European Council has endorsed a binding EU target of an at least 40% domestic reduction in greenhouse gas emissions by 2030 compared to those in 1990 [3]. In addition, the EU has proposed to increase the share of renewable energy to 27% by 2030 [3]. In this scenario, solar thermal energy is certainly part of a solution because it can provide the hot water needed for domestic water heating, the heating and refrigeration of buildings [4], and because of the low temperature requirements for building thermal applications ($< 100^{\circ}\text{C}$) [5].

The complexity of today's urban settings affects the accessibility of solar energy in the built environment [6]. The roofs of urban buildings are a logical location for solar thermal technologies, as it reduces the possibility of shading by adjacent buildings, vegetation,

or other sources of shadow. Nonetheless, it is far from optimal due to the constraints created by the number, height, construction typologies, orientation, inclination, location, shading, and building components (chimneys, elevator machine rooms, fans and plumbing vents). In this context, the available roof area has in fact been identified as one of the main limiting factors in achieving zero energy buildings, especially for the higher ones [7].

Different types of solar thermal technologies can be used in the building industry. Nonconcentrating collectors include: solar air collectors, flat-plate collectors, and evacuated tube collectors. Concentrating collectors comprise: parabolic trough collectors, and linear Fresnel reflectors. Small-scale linear Fresnel reflectors (SSLFRs) can cover a wider range of temperatures than non-concentrating collectors, and a similar range of temperatures to those of parabolic trough collectors. SSLFRs have lower efficiency and a lower cost than parabolic trough collectors. Accordingly, SSLFRs are providing a solution for cost-effective solar energy collection for the building sector.

The importance of this study lies in the possible applications of SSLFRs as, for instance: domestic water heating [8–10], heating/cooling systems of buildings [11–13], absorption of cooled air Solar-GAX cycle [14], the industrial sector [15–17], and fiber daylighting systems [18].

An SSLFR is composed of six main blocks: the fixed structure, the mobile structure, the primary and secondary reflector systems, transmission systems and the tracking system (see Fig. 1 for clarity).

* Corresponding author.

E-mail address: bayon@uniovi.es (L. Bayón).

Nomenclature

A	Mirror Field Area (m^2)	n	Number of mirrors at each side of the central mirror
AR	Area ratio	O_r	Roof orientation ($^\circ$)
A_T	Total mirror field area (m^2)	Q	Total power absorbed (W)
$A_{eff\ i}$	Effective area of the absorber tube (m^2)	W	Mirror field width (m)
A_r	Available roof area (m^2)	W_M	Mirror width (m)
a	Length of the available roof area (m)	W_{ai}	Width illuminated on the absorber by the i -th by mirror (m)
b	Width of the available roof area (m)	α_b	Absorptivity of the material of which the absorber tube is made
CL_g	Cleanliness factor of the glass	α_i	Angle between the vertical at the focal point and the line connecting the center point of each mirror to the focal point ($^\circ$)
CL_m	Cleanliness factor of the mirror	α_S	Height angle of the Sun ($^\circ$)
D	Diameter of the absorber tube (m)	β_a	Angle between the absorber tube and the horizontal plane ($^\circ$)
DNI	Direct Normal Irradiance (W/m^2)	β_i	Tilt of i – th mirror ($^\circ$)
d	Separation between two consecutive mirrors (m)	β_M	Angle between the mirror axis and the horizontal plane ($^\circ$)
E	Total annual energy (MWh)	γ_S	Azimuth of the sun ($^\circ$)
e_b	Distance between the terrace boundary and the SSLFRs, x-axis (m)	η_{opt}	Optical efficiency (%)
e'_b	Distance between the terrace boundary and the SSLFRs, y-axis, (m)	θ_i	Angle between the normal to the mirror and the angle of incidence of the sun ($^\circ$)
e_h	Transversal maintenance distance (m)	θ_L	Lateral incidence angle ($^\circ$)
e_v	Longitudinal maintenance distance (m)	θ_t	Transverse incidence angle ($^\circ$)
F_r	Roof form	θ_z	Zenith angle of the Sun ($^\circ$)
f	Height of the receiver (m)	λ	Latitude angle ($^\circ$)
H_r	Available roof height (m)	μ	Angle between the reflected ray and the normal to the NS axis ($^\circ$)
IAF	Incidence angle modifier	ρ	Reflectivity of the primary mirrors
L	Reflector length (m)	τ	Transmissivity of the glass
L_M	Length of the mirrors (m)		
L_a	Length of the single absorber tube (m)		
L_a^l	Left length of the single absorber tube (m)		
L_a^r	Right length of the single absorber tube (m)		
N	Number of reflectors		

The fixed structure rests on a custom-made foundation and serves as support for the mobile structure and the secondary reflector system. The latter is set above the mobile structure, which serves as support for the primary reflector system and allows this system to rotate on the East-West axis. The primary reflector system is composed of several stretched rows of mirrors mounted on specially designed frames. These rows can rotate on the North-South axis, so that they can follow the sun's daily movement. The secondary reflector system is composed of: an absorber tube, a cavity receiver, an insulator, and a glass cover. It is placed longitudinally above the rows of mirrors. It has a specific coating which increases its capacity to absorb the incident solar radiation. The absorber tube is encased in a cavity receiver to reduce convective heat losses. The cavity receiver is sealed within the glass cover. The concentrated solar energy is transferred through the absorber tube into some thermal fluid which remains liquid at high temperatures. Finally, the secondary reflector system can also rotate on the East-West axis.

Therefore, the position of the mirrors and the absorber tube can be adjusted using three different movements, so that the rows of mirrors reflect the sunlight to the focal line of the absorber tube optimally. These movements are achieved by means of the transmission systems and the tracking system. A prototype with these characteristics has been built at a vocational training school (CIFP-Mantenimiento y Servicios a la Producción) in La Felguera, Asturias, Spain. A patent application for this prototype has been filed with the Spanish Patent and Brand Office [19].

In this paper, we present a new methodology using several mathematical algorithms to determine the geometrical parameters and optimal distribution of SSLFRs for their installation on flat roofs

of urban buildings. The methodology has five steps. The first step consists in establishing the problem characteristics, which enables the correct choice of the packing algorithm. The second step is a parametric study that allows us to identify the parameters prone to vary between certain limits. In the third step, various types of packing algorithms are studied and used to determine and maximize the total mirror field area and likewise maximize the energy obtained on the roofs of urban buildings. In the fourth step, the appropriate sizing of the SSLFR is calculated using specific techniques on the nonlinear programming problem, which minimize the cost of each SSLFR. We also develop another algorithm intended to minimize the losses of the absorber tube. Finally, the fifth step verifies that the algorithm used is optimal.

The paper is organized as follows. The description of the engineering problem is presented in Section 2, which also summarizes the main parameters of an SSLFR and the flat roofs of urban buildings. The proposed methodology is outlined in Section 3, and the steps that integrate it are set out. Simulation results are presented in Section 4 for different scenarios, while in Section 5, a discussion of the results is performed. Finally, Section 6 summarizes the main contributions and conclusions of the paper.

2. Description of the engineering problem

This section describes the engineering problem of determining the geometrical parameters and the number of SSLFRs for their installation on flat roofs of urban buildings by means of packing algorithms.

This engineering problem is contextualized within the pertinent European legislation and the available flat roof area. European

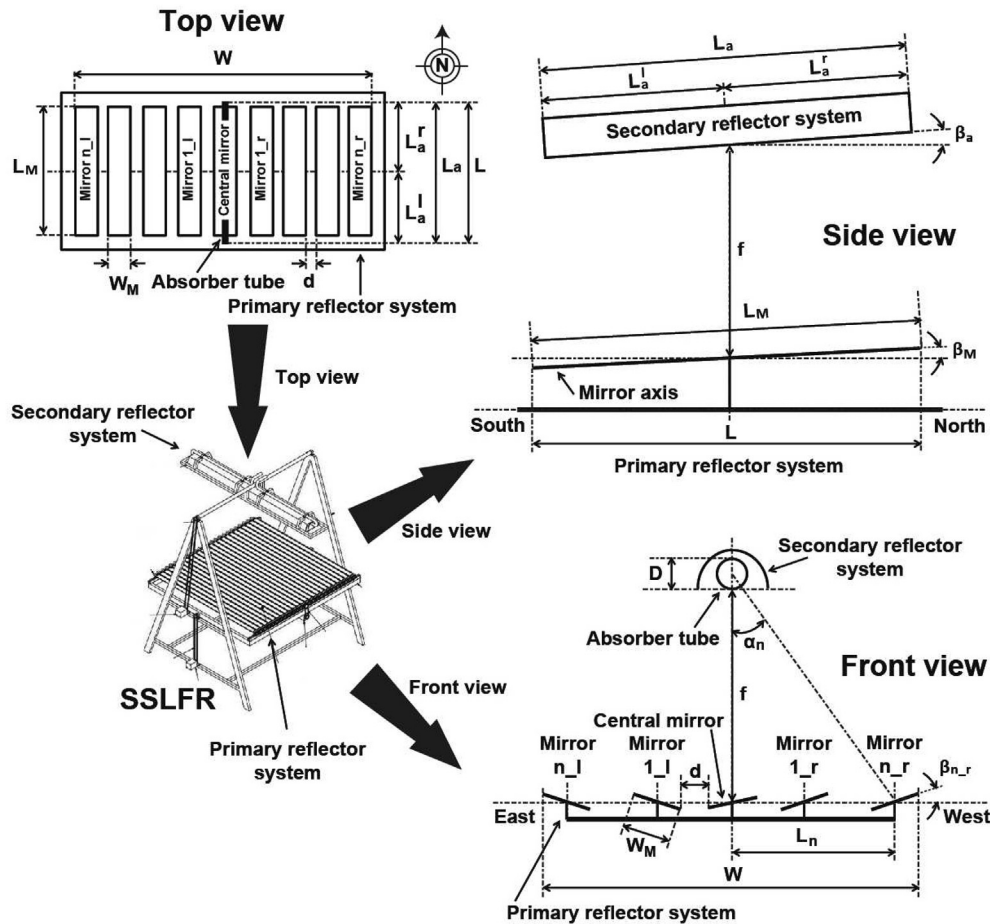


Fig. 1. SSLFR: top view, side view and front view.

legislation requires new buildings to obtain part of the energy needed for the hot water service from solar sources. Directive 2009/28/EC [20] implements the promotion of the use of energy from renewable sources. The Commission Communication established a policy framework for climate and energy in the period from 2020 to 2030 [21]. And the Directive 2018/2001/EC [22] establishes numerous requirements concerning the use of renewable energy in new and renovated buildings. The required amount of energy is calculated depending on the climate zone and the total hot water demand. The installation surface of the SSLFR is a critical parameter when working on rooftops, contrary to what occurs when working with Concentrated Solar Power.

The main geometrical parameters that define the SSLFR are listed in Table 1. As to the parameters related to the SSLFR, previous studies have covered the relationship between these parameters [23,24]. Fig. 1 shows these parameters. In addition to these parameters intrinsic to SSLFRs, it is necessary to bear in mind the parameters intrinsic to the flat roof and the parameters that affect both.

The main geometrical parameters that define the flat roof are listed in Table 2. Fig. 2 shows these parameters.

The available roof area (A_r) is the area that can be used for the installation of SSLFRs. Operating with parameters a and b , one can obtain the parameter corresponding to the form of the roof area (F_r). This parameter is defined as the ratio between length (a) and width (b). The available roof height (H_r) is defined as the height on the roof that can be used for the installation of SSLFRs. The roof

orientation (O_r) is defined by the angle that forms the north-south direction and the terrace edges.

Finally, we have to consider some other parameters, such as those that relate the SSLFRs to one another, and those that relate the SSLFRs with the flat roof, such as the transversal distance between SSLFRs (e_h), the longitudinal distance between SSLFRs (e_v), the distance between the terrace boundary and the SSLFRs, x-axis, (e_b), and the distance between the terrace boundary and the SSLFRs, y-axis, (e_b').

Thus, when such a high number of parameters need to be considered, it might be difficult for technicians to optimize the choice of the values of the engineering problem.

The following assumptions are made in this study:

- (i) Mobile structure. In this system, the tracking error and misalignment are not considered.
- (ii) Primary reflector system. The pivoting point of each mirror coincides with the central point of the mirror; hence, it is always focused on the central point of the absorber tube. The mirrors are flat and specularly reflecting. The mirrors have the same length and width.
- (iii) Secondary reflector system. A single absorber tube is used.
- (iv) Transmission systems. The tracking error and misalignment are not considered in these systems.
- (v) Tracking system. The mobile structure, secondary reflector system, and primary reflector system are perfectly tracked so that they follow the apparent movement of the Sun.

Table 1
Main geometrical parameters of an SSLFR.

	Parameters	Study
n	Number of mirrors at each side of the central mirror	Transversal
W_M	Mirror width	Transversal
d	Separation between two consecutive mirrors	Transversal
D	Diameter of the absorber tube	Transversal
f	Height of the receiver	Transversal
β_M	Angle between the mirror axis and the horizontal plane	Longitudinal
β_a	Angle between the absorber tube and the horizontal plane	Longitudinal
L_M	Mirror length	Longitudinal
L_a	Total length of the single absorber tube	Longitudinal
L_a^l	Left length of the single absorber tube.	Longitudinal
L_a^r	Right length of the single absorber tube	Longitudinal

Table 2
Main geometrical parameters of a flat roof.

	Parameters
A_r	Available flat roof area
a	Length of the available flat roof area
b	Width of the available flat roof area
H_r	Available roof height
F_r	Form of the roof
O_r	Roof orientation

3. Methodology

This paper proposes a new methodology for determining the geometrical parameters and the number of SSLFRs to be installed on flat roofs of urban buildings.

The methodology includes five steps to identify the required number of SSLFRs and their geometrical parameters to minimize cost and maximize the energy absorbed by the absorber tube. A general block diagram outlining the proposed methodology is shown in Fig. 3. The first step of the methodology consists in establishing the problem characteristics in order to examine the installation details, which comprises a certain number of requirements so that it fulfills the needs of the system. The second step of the procedure consists of a parametrical analysis, which searches for the parameters that can be bounded between upper and lower bounds. The third step searches for the packing algorithms that meets the criteria set in the first step and that maximize the total mirror field area. The fourth step of the procedure is the

choice of the SSLFR parameter values, with a double aim: on one hand, to minimize the total cost of the system, and on the other, to minimize the losses of the absorber tube. The fifth step is to verify that the chosen algorithm and the parameter values are the optimal ones by means of the determination of the total annual energy obtained.

3.1. Step 1: establishment of the problem characteristics

The specific type of two-dimensional rectangle packing problem that is addressed in this paper has the following characteristics:

- (i) One single flat roof of an urban building of fixed length and width.
- (ii) The flat roof of urban buildings are rectangular or square shaped. The shape is defined by the length (a) and width (b) of the available roof area. That area can be expressed as:

$$A_r = a \cdot b \tag{1}$$

- (iii) The flat roof of urban buildings may have an orientation angle.
- (iv) There is a set of identical SSLFRs. The dimensions of the SSLFRs are not fixed, but they are bounded between upper and lower bounds.
- (v) All the SSLFRs are rectangular or square shaped. The shape is defined by the reflector area, and can be calculated as:

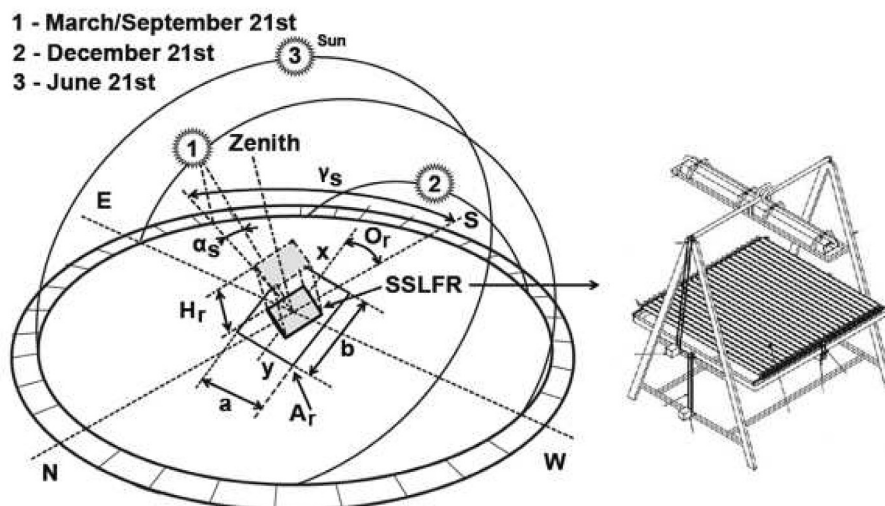


Fig. 2. Definition of roof parameters.

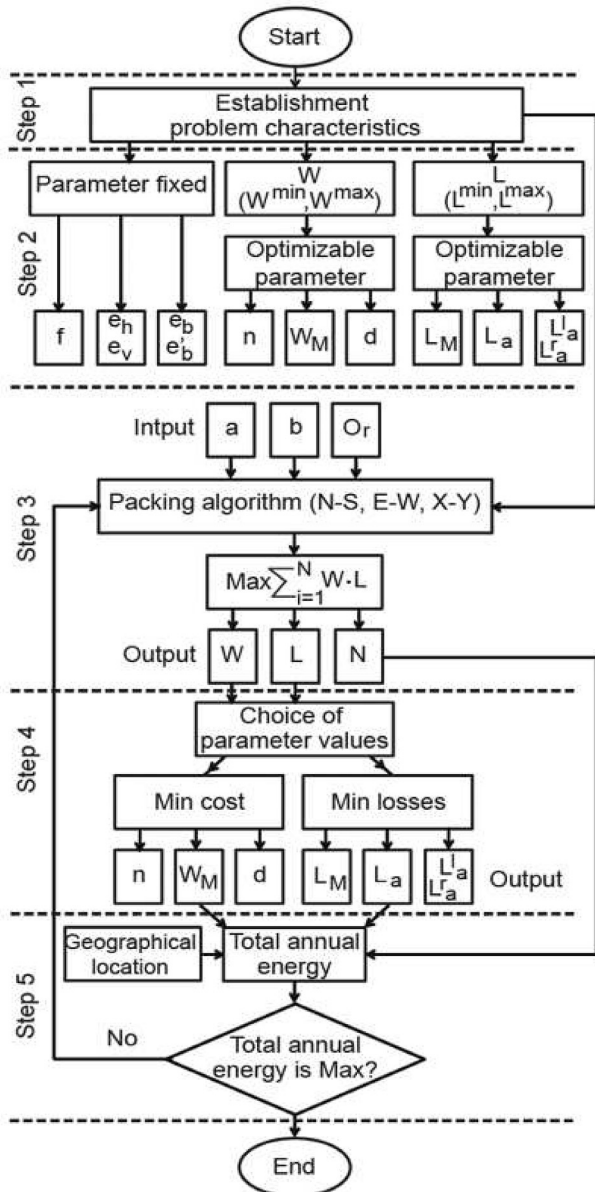


Fig. 3. A general block diagram outlining the proposed methodology.

$$A = W \cdot L \tag{2}$$

where A is the reflector area (m^2), W is the mirror field width (m), and L is the reflector length (m).

The mirror field width can be calculated as:

$$W = 2 \cdot n \cdot (W_M + d) + W_M \tag{3}$$

where n is the number of mirrors at each side of the central mirror, W_M is the mirror width (m), and d is the separation between two consecutive mirrors (m).

The reflector length can be computed using one of the following 3 laws, depending on whether the projection of the absorber tube lies inside the projection of the primary field of mirrors, or if either it overflows on the left or it overflows on the right.

- (1) If $L_a^l \cdot \cos(\beta_a) \leq \frac{1}{2} \cdot L_M \cdot \cos(\beta_M)$ and $L_a^r \cdot \cos(\beta_a) \leq \frac{1}{2} \cdot L_M \cdot \cos(\beta_M)$ then:

$$L = L_M \cdot \cos(\beta_M) \tag{4}$$

- (2) If $L_a^l \cdot \cos(\beta_a) > \frac{1}{2} \cdot L_M \cdot \cos(\beta_M)$ and $L_a^r \cdot \cos(\beta_a) \leq \frac{1}{2} \cdot L_M \cdot \cos(\beta_M)$ then:

$$L = L_a^l \cdot \cos(\beta_a) + \frac{1}{2} \cdot L_M \cdot \cos(\beta_M) \tag{5}$$

- (3) If $L_a^l \cdot \cos(\beta_a) \leq \frac{1}{2} \cdot L_M \cdot \cos(\beta_M)$ and $L_a^r \cdot \cos(\beta_a) > \frac{1}{2} \cdot L_M \cdot \cos(\beta_M)$ then:

$$L = \frac{1}{2} \cdot L_M \cdot \cos(\beta_M) + L_a^r \cdot \cos(\beta_a) \tag{6}$$

In these formulas, L_M is the mirror length (m), L_a^l is the left length of the single absorber tube (m), L_a^r is the right length of the single absorber tube (m), β_M is the angle between the mirror axis and the horizontal plane ($^\circ$), and β_a is the angle between the absorber tube and the horizontal plane ($^\circ$).

- (vi) The longitudinal position and length of the absorber tube are critical parameters for the study of an SSLFR. Using non-optimal values leads to decreases of up to 80% in the energy produced [25].
- (vii) The parameter f is limited by the available roof height, H_r .
- (viii) The SSLFR is aligned horizontally with the roof and the absorber tube is aligned in a north-south orientation. The orientation of the SSLFRs is fixed with respect to the flat roofs of urban buildings and, in general, they are not orthogonal.
- (ix) A minimum space between SSLFRs is required for maintenance purposes and to avoid shadowing effects.
- (x) A minimum space between the terrace boundary and the SSLFRs is required for maintenance purposes.

3.2. Step 2: Parametric analysis

The required volume of an SSLFR depends on the following parameters: n , W_M , d , f , D , L_M , L_a , L_a^l , and L_a^r .

3.2.1. Parameter f

The Spanish Technical Building Code [26] provides a set of instructions for the determination of H_r . According to this code, the installation of solar thermal technologies on flat roofs must meet the following requirements: i) the solar thermal device are to be placed in the center of the envelope formed by imaginary planes placed at 45° drawn from the edges of the last slab and a horizontal plane located at a height of 3.75 (m); and, ii) this installation cannot be unsightly. Therefore, the parameters f and H_r are related by the following equation:

$$(f + D + L_a^r \cdot \sin(\beta_a)) \leq H_r \tag{7}$$

Several authors, such as [25,27], use $f = 1.5$ (m) in their papers. Increasing f induces competing effects, such as losses in focusing accuracy, which tend to reduce the collector's optical efficiency. Working with $\beta_a = 45^\circ$ is the worst scenario possible. Therefore, the following expression is always true:

$$(f + D + L_a^r \cdot \sin(\beta_a)) < 3.75(m) \tag{8}$$

According to which, the parameter will always take a value of 1.5 (m).

3.2.2. Parameters n , W_M , and d

The parameters n , W_M , and d can be related to W by means of Equation (3). Parameter W is considered to be bounded between upper and lower bounds, (W^{\min} , W^{\max}), as it affects parameter A .

3.2.3. Parameters L_M , L_a , L_a^l , and L_a^r

The parameters L_M , L_a , L_a^l , and L_a^r can be related to L by means of Equations (4)–(6). Parameter L is considered to be bounded between upper and lower bounds, (L^{\min} , L^{\max}), as it also affects parameter A .

3.2.4. W and L limits

As a first approximation, the following limits were considered: $1.0 \leq W \leq 2.5$ (m) and $1.0 \leq L \leq 2.5$ (m). Other design values were not taken into account as they notably increased the cost or differ from the normal values of an SSLFR.

3.2.5. Parameters e_h , e_v , e_b , and e'_b

The Spanish Government Technical Report [30] states that, in order to minimize shadowing effects, the distance between reflectors has to guarantee a minimum of 4 h of sunshine around noon on the winter solstice. In Ref. [29], applying this standard, on December 21 at 10 : 00 am, one can determine the transversal shadow, obtaining a value of 0.782 (m) using similar parameters to those stated in this paper. In the aforementioned paper, the longitudinal shadow between SSLFRs is also determined. For this reason, we will use $e_h = e_v = 1.0$ (m). This dimension is considered suitable for maintenance purposes, and sufficient to minimize shadowing effects. Likewise, for maintenance purposes, we will consider $e_b = e'_b = 1.0$ (m).

3.3. Step 3: Maximize the total mirror field area

In step 3, the suitable types of algorithms that meet the required characteristics are selected to maximize the total mirror field area.

Packing axis-aligned rectangles in a rectangular container is the goal of several classic optimization problems. A collection of types of rectangle packing problems is reviewed in Ref. [31]: the strip packing problem, area minimization problem, two-dimensional bin packing problem, two-dimensional knapsack problem, two-dimensional cutting stock problem, and pallet loading problem. Several solutions have been proposed for these packing problems [32–36].

We have to pack identical rectangles (or squares) (A) in a fixed rectangle (or square) container (A_r) taking into account the additional constraints mentioned in the previous section: (iii), (v), (ix), and (x). The algorithm must find the reflector dimensions (W and L) which maximize the total mirror field area. Therefore, the objective function to be maximized is the total mirror field area (A_T), given by:

$$\max A_T = \max \sum_1^N W \cdot L \tag{9}$$

where N is the number of SSLFRs, W is the mirror field width, and L is the reflector length.

After searching in the specialized literature, we found three algorithms that meet the required conditions of this problem. These three algorithm are represented in Ref. [29], where they are defined by the authors as: the N–S alignment algorithm, E-W alignment algorithm, and X–Y alignment algorithm.

The type (I) N–S alignment algorithm consists in placing rows of SSLFRs parallel to the north-south direction. Starting out from each SSLFR in the first row, new SSLFRs are added in a direction parallel to

the N–S direction, using several relationships. The packing pattern is completed by placing new SSLFRs vertically aligned with the first SSLFR.

The type (II) E-W alignment algorithm consists in placing rows of reflectors parallel to the east-west direction. Starting out from each SSLFR in the first row, new SSLFRs are added in a direction parallel to the E-W direction, using several relationships. The packing pattern is completed by placing new SSLFRs horizontally aligned with the first SSLFR.

The type (III) X–Y alignment algorithm consists in placing rows of SSLFRs parallel to the terrace edges and, therefore, parallel to our reference axes ($x - y$).

The input data for the algorithms is: the length of the available flat roof area, the width of the available flat roof area, and the roof orientation.

The output data for the algorithms is: the mirror field width, the reflector length, and number of SSLFRs. These parameters will subsequently be analyzed in Step 4.

3.4. Step 4: Choice of parameter values

The sizing procedure is performed by analyzing the SSLFR parameters in order to develop an optimal configuration. The optimal values for W and L obtained in the previous step must be used so as to obtain an SSLFR configuration that ensures the minimum cost.

3.4.1. Parameters L_M , L_a , L_a^l , and L_a^r

The algorithm proposed by Ref. [24] will be used to determine the optimal values of L_a , L_a^l , and L_a^r . This algorithm allows the optimization of the position and length of the absorber tube based on the longitudinal design. This method is based on a geometrical algorithm that minimizes the area between two curves, thereby minimizing the end loss and reflected light loss, which are now taken into consideration.

Different configurations can be analyzed for the SSLFR. In this paper, we use the C_9 configuration of [24], where the rays reflected by the mirrors in the longitudinal direction are always vertical at any time of the day. According to that reference, for the C_9 configuration, we obtain:

$$L_a = L_M, \text{ and } L_a^l = L_a^r = \frac{L_a}{2} \tag{10}$$

Therefore, the optimal value for L obtained in step 3 is:

$$L = L_M = L_a \tag{11}$$

3.4.2. Parameters n , W_M , and d

The number of mirrors, ($2 \cdot n + 1$), is the parameter that most influences the cost of an SSLFR [28]. It is interesting that n remains within adequate limits so as not to increase the cost of the SSLFR. It has been proven in Ref. [23] that $n = 12$ is an adequate value. For the sake of convenience, this parameter will vary around that value.

The parameter W_M affects the width on the absorber tube illuminated by the $i - th$ mirror (W_{ai}) is given by:

$$W_{ai} = W_M \cdot [\cos \beta_i \pm \sin \beta_i \tan \alpha_i]; \quad 0 \leq i \leq 2n \tag{12}$$

where α_i is the angle between the vertical at the focal point and the line connecting the center point of each mirror to the focal point and β_i is the tilt of the $i - th$ mirror. The sign \pm must be adopted according to the following criteria: $-$ for the left side, and $+$ for the right side. The angle α_i can be calculated as:

$$\alpha_i = \arctan \left[\frac{i \cdot (W_M + d)}{f + D/2} \right]; \quad 1 \leq i \leq n \quad (13)$$

The length of the circumference on the absorber tube (l_{ai}) illuminated by the i – th mirror for $0 \leq i \leq 2n$ can be calculated as:

$$l_{ai} = \begin{cases} \frac{\pi D}{2} & \text{if } W_{ai} \cos \alpha_i > D \\ D \arcsin \left(\frac{W_{ai}}{D} \right) & \text{if } W_{ai} \cos \alpha_i \leq D \end{cases} \quad (14)$$

W_{ai} directly affects the design of the absorber cavity and, therefore, the secondary reflector system. This is the second most costly component of the SSLFR [28]. A notable increase in W_{ai} results in an increase of the aperture of the absorber cavity and the diameter of the absorber tube. Therefore, we shall consider the parameter W_M to vary around 0.060 (m). This value has been used in the designs of several authors such as [25,27].

By applying ‘Mathur’s method’ ([37,38]), we can calculate the appropriate value of the shift between adjacent mirrors, so that shading and blocking of reflected rays are avoided for a transversal incidence angle between -22.5° and 22.5° . According to ‘Mathur’s method’ the relationship between W_M and d is:

$$d = 0.075 \cdot W_M \quad (15)$$

For $W_M = 0.060$ (m), the resulting value of d is really small, leading to a significant increase in difficulties in the assembly stage of the SSLFR [28] and an increase of the wind force on primary reflector system. It would thus be necessary to reinforce the fixes and mobile structure, the movement unit, the mirror unit, the tracking system, and the foundation. Therefore, in this study we consider $d = 0.024$ (m) to avoid those inconveniences. This will also diminish the effects of shading and blocking. This value of d has been previously used in several studies [23–25].

The methodology proposed in Ref. [28] is now applied to obtain the total primary cost. For a better comprehension, the main parameters are presented in Annex I. Following this methodology, the primary cost has been divided into eight elements, as in Table A1 (from now on, all costs are given in €). In it, the respective primary costs of the elements are denoted by: C_{FS} for the fixed structure, C_{MS} for the mobile structure, C_{MoS} for the mirror system, C_{MIS} for the movement system, C_{SRS} for the secondary reflector system, C_{TS} for the tracking system, C_A for the assembly works, and C_F for the foundation. The total primary cost C_T of an SSLFR is given by the sum of these eight components:

$$C_T = C_{FS} + C_{MS} + C_{MoS} + C_{MIS} + C_{SRS} + C_{TS} + C_A + C_F \quad (16)$$

In Table A2, we present the independent variables of each component. In Table A3 we present a summary of the main required values. For the rest of parameters we refer the reader to Ref. [28]. After some computations, we found that the total cost is a non-linear function of only two independent variables, W_M , and n :

$$C_T = C_T(W_M, n) \quad (17)$$

Thus, the problem consists in the minimization of a non-linear function of two variables, $C_T(W_M, n)$, where W_M is the width of the mirrors and n their number. However, these two variables are related by a non-linear equality restriction, because the optimal value for W obtained in step 3 must be used as a constraint to obtain the values of W_M and n . Substituting d in (3), we must impose that:

$$W = 2 \cdot n \cdot (W_M + 0.024) + W_M \quad (18)$$

Determining the minimum of $C_T(W_M, n)$ is also required. This minimum lies in some specific subset of \mathbb{R}^2 : a bounded rectangular region, delimited by the minimum and maximum values of W_M and n . Finally, one of the variables, W_M is continuous (i.e. its values are real numbers) but the other one, n , the number of mirrors, is discrete. In summary, the optimization problem is a Mixed-Integer Non-Linear Programming (MINLP) problem:

$$\left. \begin{aligned} \min_{\mathbf{x}, \mathbf{y}} J(\mathbf{x}, \mathbf{y}) \\ \mathbf{h}(\mathbf{x}, \mathbf{y}) = 0 \\ \mathbf{g}(\mathbf{x}, \mathbf{y}) \leq 0 \\ \mathbf{x} \in \mathbb{R}^n, \mathbf{y} \in \mathbf{Z} \end{aligned} \right\} \rightarrow \left. \begin{aligned} \min_{W_M, n} C_T(W_M, n) \\ f(W_M, n) = W \\ W_M^{\min} \leq W_M \leq W_M^{\max}; n^{\min} \leq n \leq n^{\max} \\ W_M \in \mathbb{R}; n \in \mathbf{Z} \end{aligned} \right\} \quad (19)$$

Using the so-called Karush-Kuhn-Tucker (KKT) conditions, it is possible to find necessary conditions for the optimum solution of these problems. We also need to combine real-valued optimization with the search of integer solutions.

3.5. Step 5: Verify the choice of parameter values

After all the SSLFR parameters have been optimally dimensioned as described above, the chosen combination will be used to determine the total annual energy obtained. The power absorbed by the absorber tube of an SSLFR can be calculated as [24]:

$$Q = \sum_{i=0}^{2 \cdot n} DNI \cdot \eta_{opt} \cdot IAM_i \cdot A_{effi} \quad (20)$$

where:

- (i) DNI is the direct normal irradiance.
- (ii) η_{opt} is the total optical yield, which is calculated considering the reflectivity of the mirrors (ρ), the cleanliness factors of the mirror (Cl_m) and of the glass covering the secondary absorber (Cl_g), the transmissivity of this glass (τ), and the absorptivity of the material of which the absorber tube is made (α_b). η_{opt} can be calculated as:

$$\eta_{opt} = (\rho \cdot Cl_m) \cdot (\tau \cdot Cl_g \cdot \alpha_b) \quad (21)$$

Although some of these parameters, especially τ , should change with the angle of incidence (see Ref. [39]), they are considered constant in this study for the sake of simplicity (see Refs. [40,41]). These values are: $\rho = 0.94$ (see Ref. [39]); $Cl_m = Cl_g = 0.98$ (see Ref. [42]); $\tau = 0.87$ if $\alpha_i \leq 20^\circ$, $\tau = 0.85$ if $20^\circ \leq \alpha_i \leq 30^\circ$ (see Ref. [43]).

- (iii) IAM_i expresses the variation in the optical performance of an SSLFR for varying ray incidence angles, for the i – th mirror [25]:

$$IAM_i = \left[C_L^2 + C_{Ti}^2 + 2 \cdot C_L \cdot C_{Ti} \cdot \cos \widehat{C_L C_{Ti}} \right]^{1/2}; \quad 0 \leq i \leq 2n$$

$$C_L = \cos \gamma_S \cdot \cos \theta_L; \quad C_{Ti} = \frac{\cos \alpha_S \cdot \sin \gamma_S \cdot \cos \theta_i}{\sin \theta_t}; \quad 0 \leq i \leq 2n$$

- (iv) A_{effi} is the effective area of the absorber tube that is actually illuminated by the i – th mirror [25].

In this last step we shall check that this choice produces the maximal power Q compared to the other possible combinations.

3.6. Economic comparison

The economic comparison of our study can be carried out by estimating the levelized cost of energy *LCOE*: the present value of all the costs incurred during the lifetime of the *SSLFR* divided by the present value of the total amount of energy absorbed by the absorber tube. The *LCOE* is expressed as euros per kilowatt hour (€/kWh). The relevant costs usually required for estimating the *LCOE* include capital investments, cost of fuels, and operational and maintenance costs.

Several *LCOE* models exist for determining prices for renewable energy [44]. The equation proposed by *IRENA* [45] represents the most commonly used for estimating the *LCOE* of renewable energy technologies and is used by many authors [46,47]. Depending on the type of analysis, the *LCOE* equation can vary to accommodate necessary changes [48]. In the present study, we are going to use a modification of the equation proposed by *IRENA*, as we are going to use the energy absorbed by the absorber tube. This is because ours is a general study of the *SSLFR*: we do not cover a specific installation. So:

$$LCOE = \frac{\sum_{t=1}^n \frac{I_t + M_t + F_t}{(1+r)^t}}{\sum_{t=1}^n \frac{E_t}{(1+r)^t}}; \text{ with } E_t = E_0 \left(1 - \frac{DR}{100}\right)^t \tag{22}$$

where: I_t is the investment cost (the subindex t means “in year t ” everywhere), M_t is the operational and maintenance expenditure, F_t is the fuel expenditure, n is the expected lifetime of the *SSLFR*, E_t is the energy absorbed by the absorber tube, E_0 is the energy absorbed by the absorber tube in the first year of the installation, r is the real discount rate, and DR is the degradation factor.

Generally, the investment costs can be divided into direct and indirect capital costs. The direct capital cost is the sum of one-time expenses that are incurred for the purchase and installation of the *SSLFR*. The indirect capital cost is the cost associated with the design and construction of the rest of the installation. In this study we shall only consider the direct capital cost, as we are not studying a specific installation. Operational and maintenance costs represent the annual expenditures for labor, equipment, and other costs associated with operating the *SSLFR*. In our case, the fuel cost is 0.

4. Simulation results

The results of a large number of numerical simulations that were performed using a MATLAB code are presented in this section. The number of *SSLFRs*, the *SSLFR* parameters, and the total annual energy obtained are analyzed for various scenarios at one single geographic location. All the calculations are based on a sub-hourly distribution of direct normal irradiance in a specific geographic location: Almeria (Spain), with latitude 36°50'07"N, longitude 02°24'08"W and altitude 22 (m). A derived database and data integration system [49] were used to estimate the solar irradiance.

The numerical simulations were performed using a MATLAB code, which incorporates subroutines, discretized every 10 min, to calculate: DNI , mirror position, IAF_i , and A_{eff} . The effects of shading, blocking, and end loss have also been taken into account, in those hours in which they exist. We point the reader to Ref. [29] for a thorough study of these aspects. To show the application of the methodology proposed in the distribution of *SSLFRs* on flat roofs of urban buildings, the scenarios of Table 3 are considered.

The *LCOE* is estimated for an operational period of 25 years, which is the expected lifetime of the structural steel elements as per ANSI/AISC 360–10. The economic model assumptions for the parameters are: $r = 3\%$, $M_t = 250(\text{€})$ for each *SSLFR*, $DR = 10\%$ [50].

Table 3
Scenarios under study.

Available roof area A_r (m^2)	$10 \times 10, 10 \times 20, 10 \times 30, 20 \times 10, 30 \times 10$
Form of the roof area F_r	$= 1, < 1, > 1$
Roof orientation ($^\circ$)	0, 15, 30, 45, 60, 75, 90

4.1. Choice of the limits of W and L

After performing a large number of simulations for each of the algorithms, for the available roof area and roof orientation under study, the classification shown in Table 4 was obtained, which classifies the possibilities from highest to lowest energy obtained.

Fig. 4 shows the total annual energy area for the X–Y algorithm, with $A_r = 10 \times 10$ (m^2), $A_r = 10 \times 20$ (m^2) $A_r = 10 \times 30$ (m^2), and the roof orientations under study (see Table 3). Each dot represents the result of working with the different orientation angles corresponding to 0° or 90° , and its area indicates the total amount of energy obtained for the specific roof. In this figure, it is clear that the total annual energy obtained is greater when the available roof area is increased, but the most important conclusion is that the best result is obtained in all cases when working under the conditions of possibility 1.

According to Fig. 4, the best results are obtained when working with larger limits of W and L . Henceforth in this paper, we shall use the limits corresponding to possibility 1. Among the limits proposed in possibility 1, we can find the values used by Refs. [23–25,27] for their *SSLFRs*.

4.2. Output of the algorithms of step 3

In this step, the algorithms were implemented using the commercial software Mathematica™.

As an example, Fig. 5 shows the output of the Mathematica™ code for a flat roof of dimensions $a \times b = 20 \times 10$ (m), with an angle of orientation of 15° (X–Y algorithm), 45° (E–W algorithm), and 60° (N–S algorithm). In this figure, the different components of the output of the algorithm can be identified: the mirror field width, the reflector length, and the number of *SSLFRs*.

In order to choose the algorithm that will provide the best total annual energy results, the parameter (AR) is used. This parameter represents the total mirror field area divided by the total area of the terrace ratio, and it is clear that the greater AR is, the better the result will be.

$$AR = \frac{\sum_1^N W \cdot L}{a \cdot b}$$

The results of AR for each of the algorithms are shown in the charts represented in Fig. 6(a), Fig. 7(a), and Fig. 8(a). According to the information shown in the charts, there is no “winning” algorithm, as the best results are obtained using different algorithms depending on the input dimensions and orientation of the flat roof. It can be seen that for roof orientations of 0° or 90° , the result is the same regardless of the algorithm or the values of a and b . For roof orientations of 15° and 75° , the best algorithm is the X–Y alignment algorithm, though for 45° this algorithm shows the worst

Table 4
Limits of W and L .

Possibility	W^{\min} (m)	W^{\max} (m)	L^{\min} (m)	L^{\max} (m)
1	2.0	2.5	2.0	2.5
2	2.0	2.5	1.0	1.5
3	1.0	1.5	2	2.5

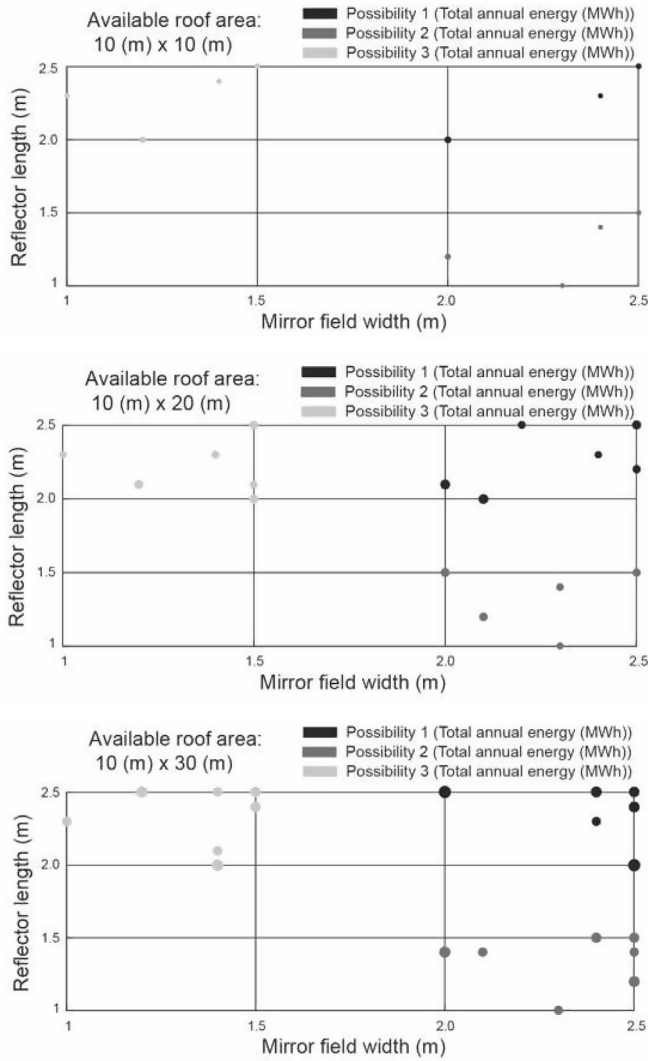


Fig. 4. Limits of W and L.

results. Similar results are obtained using different algorithms when using $a = 20$ (m) and $b = 10$ (m), or $a = 30$ (m) and $b = 10$ (m).

Figs. 6(b), 7(b) and 8(b) show the results of the number of SSLFRs for each algorithm. Generally, the best AR result matches the result with the largest number of SSLFRs. However, it may be the case that the algorithm that obtains the greatest AR does so with the lowest number of SSLFRs, due to the values of W and L . An example of this can be seen when working with: $a = 10$ (m), $b = 10$ (m), and $Or = 30^\circ$ (See Fig. 6(a) and 6(b)). This fact is very important, as the cost of the installation would also be the lowest.

4.3. Output of the algorithm of step 4

4.3.1. Step 4.1

As explained in Step 4.1, the special properties of the configuration C_9 provide, in a direct way, from the L value obtained by the packing algorithms, both the length of the mirrors and, essentially, the length of the absorber tube and its position:

$$L = L_a = L_M, \text{ and } L_a^l = L_a^r = \frac{L_a}{2} \tag{23}$$

4.3.2. Step 4.2

At this point, the output of the algorithm which minimizes the production cost of each SSLFR can be seen in detail. As we have already explained, the mathematical problem is of the MINLP type (19), where the minimal cost function is obtained from the cost parameters of the example proposed in Ref. [28], included in the Annex, and which give:

$$C_T = 2479.13 + 16031 \cdot W_M + n(141.2 + 1040.7W_M) \tag{24}$$

Notice that for the configuration C_9 , the parameter giving the number of allowed movements to the SSLFR takes the value $a = 3$ (triple movement). The equality restriction is due to the value of W obtained in step 3:

$$W = 2 \cdot n \cdot (W_M + 0.024) + W_M \tag{25}$$

As regards the inequality restrictions, we have imposed the following limits: $n^{\min} = 8$, and $n^{\max} = 17$, values around $n = 12$, which, as we have already stated, are optimal for the proposed design. Finally, recall that the variable W_M is continuous but n is integer.

By way of example, we show the solution obtained when the optimal value of W in step 3 is $W = 2$ and the length is $L = 2$. The remaining values appearing in Table 3 are obtained similarly. With those inputs, the variation range of W is between $W_M^{\min} = 0.034$ (m) and $W_M^{\max} = 0.095$ (m). Fig. 9 shows a graphical representation of the optimal point. The total cost of an SSLFR in the minimum point is 5790.97€. The optimal point corresponds to building an SSLFR with $n = 11$ mirrors and $W_M = 0.064$ (m).

Fig. 9 shows also the level curves of the function $C_T(W_M, n)$ (24), the curve representing the equality restriction (25) $W = f(W_M, n)$ and the box constraints for the independent variables $W_M^{\min} \leq W_M \leq W_M^{\max}$, $n^{\min} \leq n \leq n^{\max}$.

In our case, as we are seeking a global (and, if possible, exact) optimization, we have decided to use the Karush-Kuhn-Tucker conditions (KKT). We also combine optimization on the real numbers with the search for integer solutions. The results have been obtained using the commercial software Mathematica™.

4.4. Output of step 5

As we have already indicated, the objective of this last step is to verify whether the choice of parameters is optimal in the sense of getting the maximum power Q compared to other possible combinations. For the sake of simplicity we present in Table 5 an example. We consider the case with: $a = 10$ (m), $b = 30$ (m), and roof orientation $Or = 30^\circ$.

Notice how, among all the possible combinations of the packing algorithms, the one delivering the greatest AR is also the one producing the maximum Q . This result confirms the proposed methodology and allows us not to repeat the previous steps, which possibility was included in the flowchart of Fig. 3.

In Table 6 we show the optimum values for all the scenarios studied in this paper.

The greatest amount of total annual energy is obtained, regardless of the scenario studied or the algorithm used, for 0° and 90° . These will be used as the base values for latter comparisons with the remaining orientations.

If the flat roof of an urban building is square in shape, i.e. $a = 10$ (m) and $b = 10$ (m), as the roof orientation increases, the obtained energy decreases, approximately 32%, while the number of SSLFRs decreases approximately a 55%. When the roof orientation is 45° , the energy decreases about 28% and the number of SSLFRs required decreases approximately 45%.

If the flat roof of an urban building has a rectangular shape, i.e.

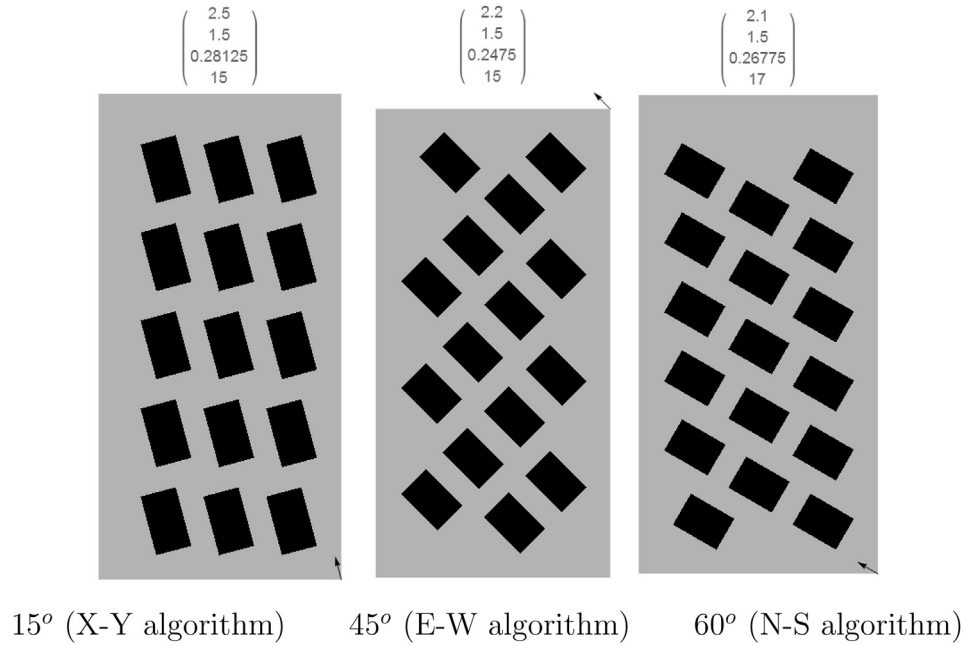
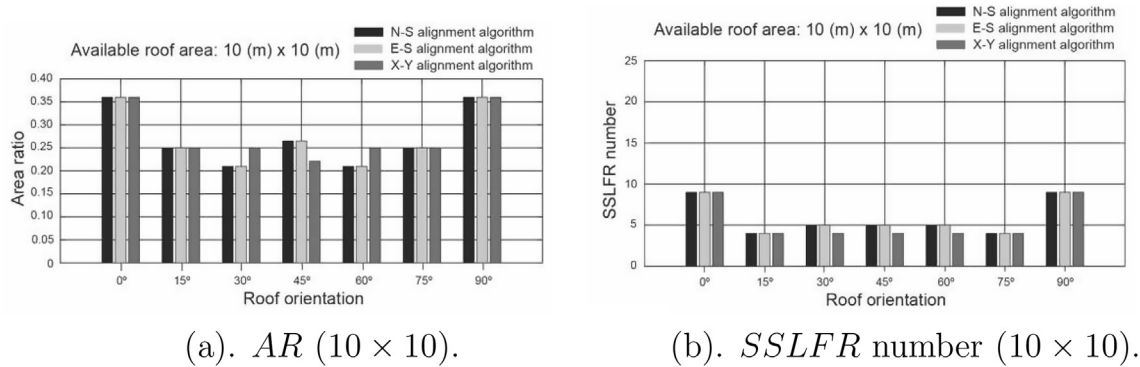


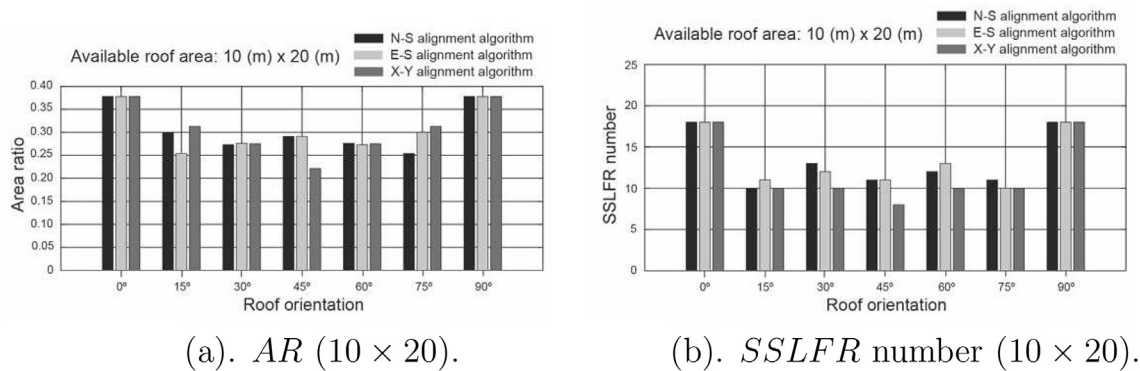
Fig. 5. Output of the Mathematica™ code.



(a). AR (10×10).

(b). $SSLFR$ number (10×10).

Fig. 6. (a). $AR(10 \times 10)$. (b). $SSLFR$ number (10×10).



(a). AR (10×20).

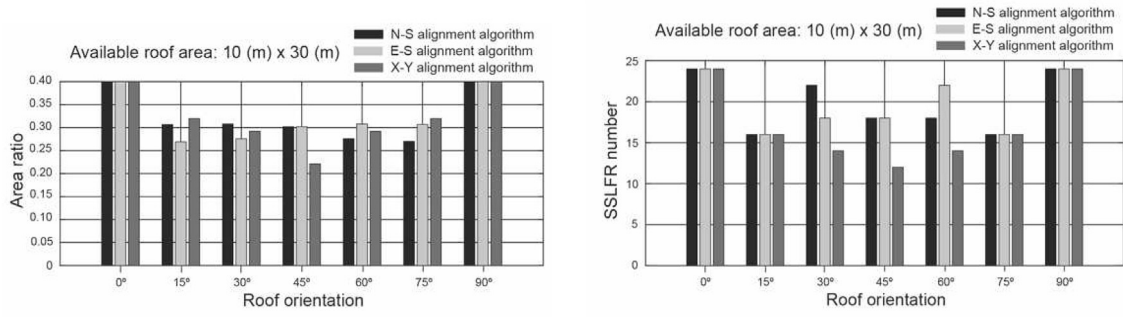
(b). $SSLFR$ number (10×20).

Fig. 7. (a). $AR(10 \times 20)$. (b). $SSLFR$ number (10×20).

$a = 10$ (m) and $b = 20$ (m), for roof orientations of 15° or 75° , the energy decreases approximately 20%, while the number of $SSLFR$ s decreases approximately 45%. When the roof orientation is 30° or 60° , the obtained energy decreases approximately 38%, while the number of $SSLFR$ s decreases about 33%. When the roof orientation

takes the value of 45° , the energy decreases approximately 25%, while the number of $SSLFR$ s decreases around 39% compared to the base value.

If the flat roof of an urban building has a more pronounced rectangular shape, i.e. $a = 10$ (m) and $b = 30$ (m), when the roof



(a). $AR (10 \times 30)$.

(b). $SSLFR$ number (10×30) .

Fig. 8. (a). $AR (10 \times 30)$. (b). $SSLFR$ number (10×30) .

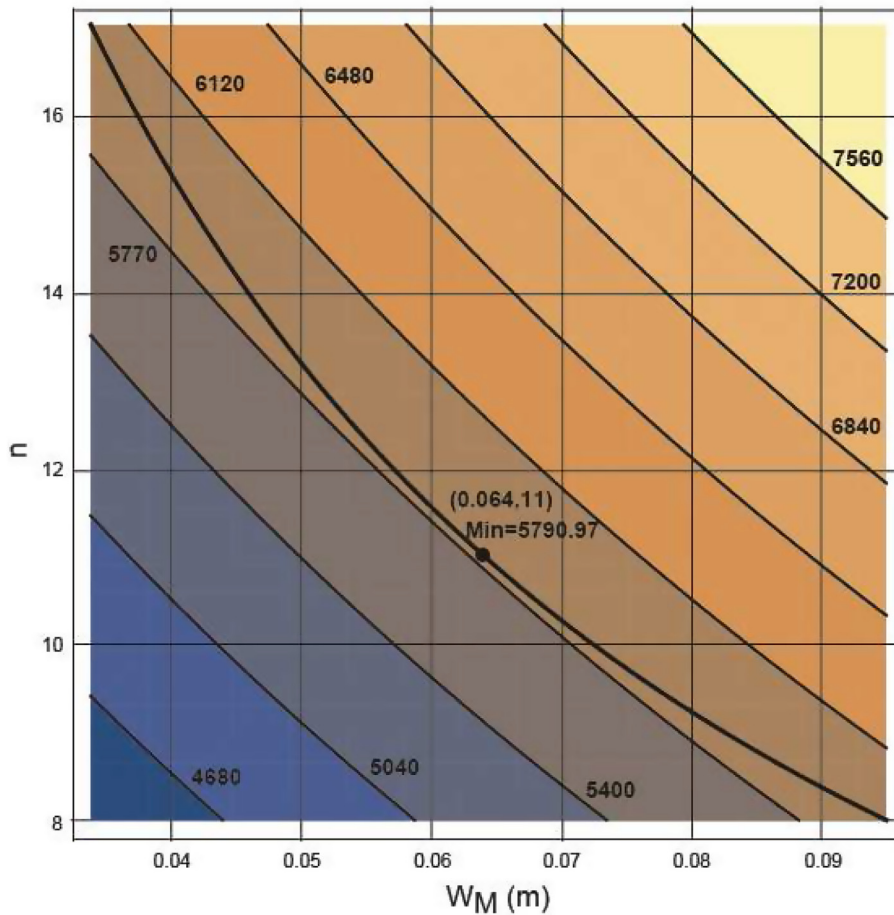


Fig. 9. Minimization of the cost: MINLP problem.

orientation is 15° or 75° , the energy obtained decreases approximately 17%, while the number of $SSLFRs$ decreases approximately 33%. When the roof orientation is either 30° or 60° , the energy decreases approximately 18%, while the number of $SSLFRs$ decreases about 9%. When the roof orientation takes the value of 45° , the energy decreases approximately 20%, while the number of $SSLFRs$ decreases about 25%.

It can be concluded that, as the rectangular shape becomes more pronounced, the decrease both in absorbed energy and in the number of $SSLFRs$ required is reduced.

The results show that the packing algorithm which provides the

best solution highly depends on the characteristics of the shape, dimensions and orientation of the roof. The greatest amount of total annual energy is obtained in the cases where the roof has a orientation of 0° or 90° , regardless of its form, the available roof area or the algorithm employed. However, the number of $SSLFR$ devices increases in these cases. When working with other orientation angles, the total annual energy obtained decreases between 17% and 33%, while the number of $SSLFRs$ decreases between 9% and 55%, depending on the available roof area.

Fig. 10 shows the solar irradiance profile for Almeria on June 21st (Summer solstice) and December 21st (Winter solstice).

Table 5
Verification of the optimal Q.

				N–S			E–W			X–Y		
W(m)	L(m)	W_M (m)	n	AR	N	E(MWh)	AR	N	E(MWh)	AR	N	E(MWh)
2.0	2.0	0.064	11	0.240	18	103.10	0.293	22	126.02	0.213	16	91.65
2.1	2.0	0.068	11	0.252	18	108.11	0.210	15	90.09	0.224	16	96.10
2.2	2.0	0.065	12	0.234	16	100.09	0.220	15	93.83	0.234	16	100.08
2.3	2.0	0.069	12	0.245	16	104.87	0.230	15	98.32	0.245	16	104.87
2.4	2.0	0.073	12	0.240	15	102.87	0.240	15	102.87	0.256	16	109.73
2.5	2.0	0.077	12	0.250	15	107.85	0.250	15	107.86	0.266	16	115.05
2.0	2.1	0.064	11	0.252	18	108.26	0.308	22	132.32	0.224	16	96.23
2.1	2.1	0.061	12	0.264	18	112.39	0.220	15	93.66	0.235	16	99.91
2.2	2.1	0.065	12	0.246	16	105.09	0.231	15	98.52	0.246	16	105.10
2.3	2.1	0.069	12	0.241	15	103.24	0.225	14	96.35	0.225	14	96.35
2.4	2.1	0.066	13	0.252	15	106.88	0.235	14	99.75	0.235	14	99.75
2.5	2.1	0.077	12	0.262	15	113.25	0.245	14	105.70	0.245	14	105.70
2.0	2.2	0.064	11	0.264	18	113.42	0.205	14	88.21	0.205	14	88.21
2.1	2.2	0.061	12	0.261	17	111.21	0.215	14	91.58	0.215	14	91.58
2.2	2.2	0.065	12	0.258	16	110.09	0.225	14	96.33	0.225	14	96.33
2.3	2.2	0.062	13	0.253	15	106.58	0.236	14	99.47	0.236	14	99.47
2.4	2.2	0.066	13	0.264	15	111.97	0.246	14	104.50	0.246	14	104.50
2.5	2.2	0.069	13	0.220	12	92.76	0.256	14	108.22	0.256	14	108.22
2.0	2.3	0.064	11	0.276	18	118.57	0.214	14	92.22	0.214	14	92.22
2.1	2.3	0.061	12	0.273	17	116.26	0.225	14	95.74	0.225	14	95.74
2.2	2.3	0.058	13	0.202	12	84.33	0.236	14	98.39	0.236	14	98.39
2.3	2.3	0.062	13	0.211	12	89.14	0.246	14	103.99	0.246	14	103.10
2.4	2.3	0.066	13	0.220	12	93.65	0.257	14	109.25	0.257	14	109.25
2.5	2.3	0.069	13	0.230	12	96.97	0.268	14	113.13	0.268	14	113.13
2.0	2.4	0.057	12	0.224	14	94.27	0.208	13	87.54	0.224	14	94.27
2.1	2.4	0.061	12	0.235	14	99.90	0.218	13	92.77	0.235	14	99.91
2.2	2.4	0.058	13	0.211	12	88.00	0.228	13	95.33	0.246	14	102.67
2.3	2.4	0.062	13	0.220	12	93.02	0.239	13	100.77	0.257	14	108.52
2.4	2.4	0.060	14	0.230	12	96.46	0.249	13	104.50	0.268	14	112.54
2.5	2.4	0.063	14	0.240	12	100.33	0.260	13	108.69	0.280	14	117.05
2.0	2.5	0.057	12	0.233	14	98.20	0.216	13	91.18	0.233	14	98.20
2.1	2.5	0.055	13	0.227	13	94.58	0.227	13	94.58	0.245	14	101.86
2.2	2.5	0.053	14	0.220	12	89.62	0.238	13	97.09	0.256	14	104.56
2.3	2.5	0.062	13	0.230	12	96.87	0.249	13	104.96	0.268	14	113.04
2.4	2.5	0.066	13	0.240	12	101.79	0.260	13	110.27	0.280	14	118.75
2.5	2.5	0.063	14	0.250	12	104.51	0.270	13	113.22	0.291	14	121.93

Finally, we show in Fig. 11, for the example of Section 4.3.2 (Step 4.2), with $n = 11$ and $W_M = 0.064$ (m), the optimal monthly total energy absorbed by the absorber tube.

5. Discussion of the results

Let us summarize the main outcomes obtained in the previous section.

5.1. Choice of the limits of W and L

According to the results, we shall use the limits corresponding to possibility 1. In possibility 2, as L decreases, the total energy obtained decreases. The reason behind this decrease in the total energy obtained is that, for smaller L , the area occupied by one SSLFR also decreases, making it possible to fit more devices on the same roof top. However, each SSLFR requires unused space for maintenance purposes and to avoid shadowing, which finally, reduces the total amount of energy absorbed. In this case, the cost of each SSLFR will most likely decrease, but, as more SSLFRs will fit in the design, the total cost reduction is not significant [28]. Possibility 3 shows a similar behavior: as W decreases, the total energy obtained also decreases, as does the unitary cost of an SSLFR. However, in order to achieve the same amount of absorbed energy as in possibility 1, the design requires installing more SSLFRs, thereby increasing the total cost of the installation.

5.2. Packing algorithms of step 3

The optimization procedure considers three packing algorithms, developed specifically for this problem by the authors. The results show that the algorithm which provides the best solution depends on the characteristics of each particular situation, i.e. the dimensions and orientation of the terrace, and the values considered for the upper and lower bounds of the reflector dimensions (width and length). So, there is no general winning algorithm. Usually, the best AR corresponds to the largest number of SSLFRs, but not always. In some cases, the algorithm obtaining the greatest AR does so with the least number of SSLFRs. This fact is very important, as this will affect the minimum total cost of installation. The question whether this parameter is the critical one for maximizing energy has been satisfactorily answered in the last step of the methodology.

5.3. Algorithms of step 4

A first algorithm allows the optimization of the position and length of the absorber tube based on the longitudinal design. It minimizes both the end loss and the reflected light loss. In this paper, we use the C_9 configuration, in which the rays reflected by the mirrors in the longitudinal direction are always vertical at any time of the day. A second algorithm is now applied to obtain the minimum of the total primary cost $C_T(W_M, n)$. It consists in the minimization of a non-linear function of two variables, W_M (the width of the mirrors) and n (their number); they are related by a

Table 6
Optimal values for the scenarios under study.

Input		Step 3				Step 4			Step 5			
a × b	Or(°)	Alg.	W(m)	L(m)	N	W _M (m)	d(m)	n	L _M (m)	E(MWh)	LCOE(€/kWh)	
10 × 10	0	ALL	2.0	2.0	9	0.064	0.024	11	2.0	51.55	0.113	
	15	ALL	2.5	2.5	4	0.063	0.024	14	2.5	34.84	0.082	
	30	III	2.5	2.5	4	0.063	0.024	14	2.5	34.84	0.082	
	45	I, II	2.3	2.3	5	0.062	0.024	13	2.3	37.14	0.092	
	60	III	2.5	2.5	4	0.063	0.024	14	2.5	34.84	0.082	
	75	ALL	2.5	2.5	4	0.063	0.024	14	2.5	34.84	0.082	
	90	ALL	2.0	2.0	9	0.064	0.024	11	2.0	51.55	0.113	
	10 × 20	0	ALL	2.0	2.1	18	0.064	0.024	11	2.1	108.26	0.109
		15	III	2.5	2.5	10	0.063	0.024	14	2.5	87.09	0.082
30		I	2.0	2.3	12	0.057	0.024	12	2.3	67.34	0.119	
45		I, II	2.3	2.3	11	0.062	0.024	13	2.3	81.71	0.092	
60		II	2.3	2.0	12	0.069	0.024	12	2.0	78.66	0.101	
75		III	2.5	2.5	10	0.063	0.024	14	2.5	87.09	0.082	
90		ALL	2.1	2.0	18	0.068	0.024	11	2.0	133.17	0.088	
10 × 30		0	ALL	2.0	2.5	24	0.051	0.024	13	2.5	160.67	0.101
		15	III	2.5	2.4	16	0.063	0.024	14	2.4	133.77	0.084
	30	II	2.0	2.1	22	0.064	0.024	11	2.1	132.32	0.109	
	45	I, II	2.4	2.1	18	0.066	0.024	13	2.1	128.26	0.095	
	60	I	2.1	2.0	22	0.068	0.024	11	2.0	132.14	0.109	
	75	III	2.4	2.5	16	0.066	0.024	13	2.5	124.86	0.091	
	90	ALL	2.5	2.0	24	0.077	0.024	12	2.0	172.57	0.094	
	20 × 10	0	ALL	2.1	2.0	18	0.068	0.024	11	2.0	133.17	0.088
		15	III	2.5	2.5	10	0.063	0.024	14	2.5	87.09	0.082
30		II	2.3	2.0	12	0.069	0.024	12	2.0	78.66	0.101	
45		I, II	2.3	2.3	11	0.062	0.024	13	2.3	81.71	0.092	
60		I	2.0	2.3	12	0.057	0.024	12	2.3	67.34	0.119	
75		III	2.5	2.5	10	0.063	0.024	14	2.5	87.09	0.082	
90		ALL	2.0	2.1	18	0.064	0.024	11	2.1	108.26	0.109	
30 × 10		0	ALL	2.5	2.0	24	0.077	0.024	12	2.0	172.57	0.094
		15	III	2.4	2.5	16	0.066	0.024	13	2.5	124.86	0.091
	30	I	2.1	2.0	22	0.068	0.024	11	2.0	132.14	0.109	
	45	I, II	2.4	2.1	18	0.066	0.024	13	2.1	128.26	0.095	
	60	II	2.0	2.1	22	0.064	0.024	11	2.1	132.32	0.109	
	75	III	2.5	2.4	16	0.063	0.024	14	2.4	133.77	0.084	
	90	ALL	2.0	2.5	24	0.051	0.024	13	2.5	160.67	0.101	

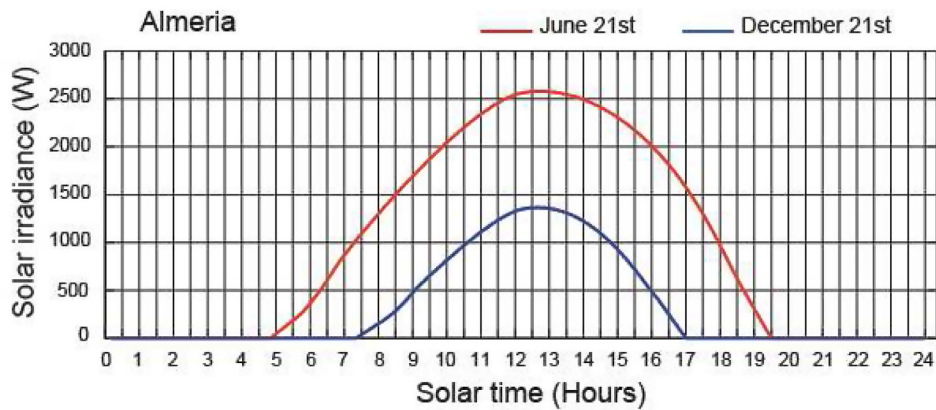


Fig. 10. Solar irradiance profile.

non-linear equality restriction. These two algorithms choose the optimizable parameters by restricting the values of W and L to those given by the previous step.

5.4. Verification of step 5

Once all the verifications are carried out (see, for instance, Table 5), we deduce that the highest values of AR always provide the greatest amount of total obtained energy. The remaining internal parameters of the $SSLFR$ (computed in step 4) are also consistent with the final objective).

6. Conclusions

This research paper presents a new methodology for determining the geometrical parameters and optimal distribution for small-scale linear Fresnel reflectors on flat roofs of urban buildings. The main distinctive feature with respect to previous studies is the integration of multiple objective functionals in the successive stages, in order to obtain, as the final objective, the maximization of the annual energy obtained. Using our technique, the decision maker can optimally choose the values of all the variables in the real problem. As a matter of fact, up to 21 variables can be considered.

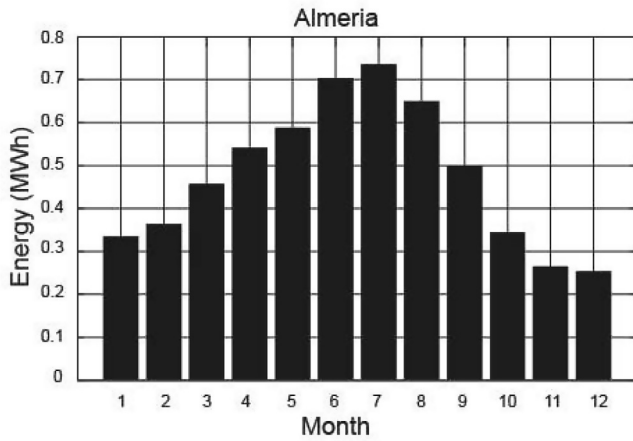


Fig. 11. Monthly total energy absorbed by the absorber tube.

We remark the following two key steps in the process: (1) In stage 3, several packing algorithms are used in order to maximize the mirror area ratio AR . This geometric parameter is shown, in the final verification, to be the optimal in order to provide the solution with the greatest amount of total annual energy. (2) In stage 4, (once AR has been maximized), two different optimization techniques are used; on one hand, the optimal values of W_M and n are

computed to minimize the cost of each reflector. On the other, the optimal values of L_M , L_a , L_a^l and L_a^r are computed to minimize the losses (end loss and reflected light loss) of the absorber tube.

Finally, we have proved that this combination of objectives, described here for the first time, attains the maximization of the energy obtained on the roofs of urban buildings. For all those reasons, we believe that this new methodology is expected to contribute to the integration of small-scale linear Fresnel reflectors on flat roofs of urban buildings.

Acknowledgments

We wish to thank M. F. Fanjul, head of the CIFP-Mantenimiento y Servicios a la Producción vocational training school in La Felguera, Asturias, Spain, and the teachers L. Rodríguez and F. Salguero for their work on the building of the prototype for the design presented in this paper.

Annex I

First, we provide the nomenclature used in the Cost Analysis. The symbol k together with the appropriate superindex represents each cost parameter, whereas an L with the appropriate superindex indicates the corresponding length and a W , the weight.

Now we show the elements defining the primary cost.

Table A.1
Primary cost.

Element	Cost
Fixed structure	$C_{FS} = W_{FS} \cdot k^{St}$
Mobile structure	$C_{MS} = W_{MS} \cdot k^{St} + L_{rail} \cdot k^R$
Movement system	$C_{MoS} = (2 \cdot n + a) \cdot k^{MoU}$
Mirror system	$C_{MiS} = (2 \cdot n + 1) \cdot k^{MiU}$
Secondary reflector	$C_{SRS} = W_{AT} \cdot k^{AT} + A_{CR} \cdot k^{CR} + A_j \cdot k^l + A_{GC} \cdot k^{GC} C_{SRS} = W_{AT} \cdot k^{AT} + A_{CR} \cdot k^{CR} + A_j \cdot k^l + A_{GC} \cdot k^{GC} + W_{SRSS} \cdot k^{St} + A_{PC} \cdot k^{PC} + L_{shaft} \cdot k^{shaft} C_{SRS}$
Tracking system	$C_{TS} = a \cdot k^{MD} + k^C + k^{Se}$
Assembly	$C_A = (2 \cdot n + a) \cdot k^A$
Foundation	$C_F = V_F \cdot k^F$

Table A.2
Cost parameters and independent variables.

Element	Cost parameters	Ind. variables
Fixed structure	$W_{FS} = W_{FS}^U \cdot L_{FS}$ $L_{FS} = 2 \cdot W_M \cdot (1 + 2.15 \cdot n) + 3 \cdot L_M + 4 \cdot \sqrt{2 \cdot \left(\frac{L_M}{2}\right)^2 + 1.5 \cdot L_M + (1.5)^2}$	W_M, L_M, n
Mobile structure	$W_{MS} = W_{MS}^U \cdot L_{MS}$ $L_{MS} = 2 \cdot (W_M \cdot (1 + 2.15 \cdot n) + L_M)$ $L_{rail} = 2 \cdot W_M \cdot (1 + 2.15 \cdot n)$	W_M, L_M, n
Movement unit	$A_{mirror} = W_M \cdot L_M$ $A_{frame} = W_M \cdot L_M$ $L_{shaft} = L_M$	W_M, L_M, L_a, f, n W_M, L_M
Secondary reflector	$W_{AT} = W_{AT}^U \cdot L_{AT} = W_{MS}^U \cdot 2 \cdot L_a$ $A_{CR} = 3.40 \cdot L_a \cdot W_M$ $A_{GC} = 2.4 \cdot L_a \cdot W_M$ $W_{SRSS} = W_{SRSS}^U \cdot (L_a + 2.4 \cdot W_M)$ $A_{PC} = 3.40 \cdot L_a \cdot W_M$ $L_{shaft} \text{ SRS} = W_M \cdot (1 + 2.15 \cdot n)$	W_M, L_M, L_a, n
Tracking system		Configuration
Assembly		W_M, L_M, f, n
Foundation		W_M, L_M, f, n

And finally, the specific data for the example.

Table A.3
Cost parameters.

Param.	Value
k^{St}	4.53 (€/kg)
k^R	29 (€/m)
k^{MoU}	53 (€/unit)
k^{mirror}	54.83 (€/m ²)
k^{frame}	103.65 (€/m ²)
$k^{shaft Mi}$	2.80 (€/m)
k^{AT}	20 (€/kg)
k^{CR}	1588 (€/m ²)
Param.	Value
k^I	50 (€/m ²)
k^{GC}	60 (€/m ²)
k^{PC}	600 (€/m ²)
$k^{shaft SRS}$	3 (€/m)
k^{MD}	212 (€)
k^C	100 (€)
k^{Se}	200 (€)
k^A	12 (€/unit)
Param.	Value
k^F	100 (€/m ³)
L_M	2.00 (m)
f	1.50 (m)
L_a	2.00 (m)
W_{FS}^U	8.96 (kg/m)
W_{MS}^U	5.19 (kg/m)
W_{SRSS}^U	1.7 (kg/m)
a	3

References

- [1] UN Treaty Collection, Kyoto Protocol to the United Nations Framework Convention on Climate Change, 1998.
- [2] Doha Amendment to the Kyoto Protocol, Adopted, Decision 1/CMP. vol. 8, 8 December 2012, C.N.718.2012.TREATIES-XXVII.7.c, 2012.
- [3] European Council Report, Last access 06/02/2019, https://www.consilium.europa.eu/uedocs/cms_data/docs/pressdata/en/ec/145397.pdf.
- [4] D.G. Gunjo, P. Mahanta, P.S. Robi, CFD and experimental investigation of flat plate solar water heating system under steady state condition, *Renew. Energy* 106 (2017) 24–36.
- [5] B. Zou, J. Dong, Y. Yao, Y. Jiang, An experimental investigation on a small-sized parabolic trough solar collector for water heating in cold areas, *Appl. Energy* 163 (2016) 396–407.
- [6] N. Mohajeri, G. Upadhyay, A. Gudmundsson, D. Assouline, J. Kämpf, J.L. Scartezzini, Effects of urban compactness on solar energy potential, *Renew. Energy* 93 (2016) 469–482.
- [7] B. Giffith, P. Torcellini, N. Long, Assessment of the Technical Potential for Achieving Zero-Energy Commercial Buildings, ACEEE Summer Study Pacific Grove, 2006.
- [8] T. Sultana, G.L. Morrison, G. Rosengarten, Thermal performance of a novel rooftop solar micro-concentrating collector, *Sol. Energy* 86 (2012) 1992–2000.
- [9] T. Sultana, G.L. Morrison, R.A. Taylor, G. Rosengarten, Numerical and experimental study of a solar micro concentrating collector, *Sol. Energy* 112 (2015) 20–29.
- [10] G. Mokhtar, B. Boussad, S. Noureddine, A linear Fresnel reflector as a solar system for heating water: theoretical and experimental study, *Case Stud. Therm. Eng.* 8 (2016) 176–186.
- [11] P. Bermejo, F.J. Pino, F. Rosa, Solar absorption cooling plant in Seville, *Sol. Energy* 84 (2010) 1503–1512.
- [12] F.J. Pino, R. Caro, F. Rosa, J. Guerra, Experimental validation of an optical and thermal model of a linear Fresnel collector system, *Appl. Therm. Eng.* 50 (2013) 1463–1471.
- [13] M.A. Serag-Eldin, Thermal design of a roof-mounted CLFR collection system for a desert absorption chiller, *Int. J. Sustain. Energy* 33 (2014) 506–524.
- [14] N. Velázquez, O. García-Valladares, D. Saucedo, R. Beltrán, Numerical simulation of a linear Fresnel reflector concentrator used as direct generator in a Solar-GAX cycle, *Energy Convers. Manag.* 51 (2010) 434–445.
- [15] R. Singh, Modeling and performance analysis of linear Fresnel collector for process heat generation for ice cream factory in Konya. MS Thesis, Middle East Technical University, 2017.
- [16] A. Häberle, M. Berger, F. Luginsland, C. Zahler, M. Baitsch, H. Henning, M. Rommel, Linear concentrating Fresnel collector for process heat applications. Solar Paces, in: 13th International Symposium on Concentrating Solar Power and Chemical Energy Technologies, June 20–23, Sevilla, Spain, 2006.
- [17] J. Rawlins, M. Ashcroft, Report: Small Scale Concentrated Solar Power – a Review of Current Activity and Potential to Accelerate Employment, carbon trust, 2013.
- [18] A. Barbón, J.A. Sánchez-Rodríguez, L. Bayón, N. Barbón, Development of a fiber daylighting system based on a small scale linear Fresnel reflector: theoretical elements, *Appl. Energy* 212 (2018) 733–745.
- [19] A. Barbón, L. Bayón, N. Barbón, J.A. Otero, C. Bayón-Cueli, L. Rodríguez, F. Salgero, Concentrador solar lineal Fresnel con triple movimiento, Spain Patent ES 2601222 (B1) (2017).
- [20] Directive 2009/28/EC, On the Promotion of the Use of Energy from Renewable Sources, 2009.
- [21] European Commission, A Policy Framework for Climate and Energy in the Period from 2020 to 2030, 2014.
- [22] Directive 2018/2001/EC, On the Promotion of the Use of Energy from Renewable Sources, 2018.
- [23] A. Barbón, N. Barbón, L. Bayón, J.A. Otero, Theoretical elements for the design of a small-scale linear Fresnel reflector: frontal and lateral views, *Sol. Energy* 132 (2016) 188–202.
- [24] A. Barbón, N. Barbón, L. Bayón, J.A. Otero, Optimization of the length and position of the absorber tube in small-scale Linear Fresnel Concentrators, *Renew. Energy* 99 (2016) 986–995.
- [25] A. Barbón, N. Barbón, L. Bayón, J.A. Sánchez-Rodríguez, Parametric study of the small-scale linear Fresnel reflector, *Renew. Energy* 116 (2018) 64–74.
- [26] Spanish Technical Building Code Royal Decree 314/2006 of 17 March 2006.
- [27] Y. Zhu, J. Shi, Y. Li, L. Wang, Q. Huang, G. Xu, Design and thermal performances of a scalable linear Fresnel reflector solar system, *Energy Convers. Manag.* 146 (2017) 174–181.
- [28] A. Barbón, J.A. Sánchez-Rodríguez, L. Bayón, C. Bayón-Cueli, Cost estimation relationships of a small scale linear Fresnel reflector, *Renew. Energy* 134 (2019) 1273–1284.
- [29] A. Barbón, N. Barbón, L. Bayón, J.A. Sánchez-Rodríguez, Optimization of the distribution of small-scale linear Fresnel reflectors on roofs of urban buildings, *Appl. Math. Model.* 59 (2018) 233–250.
- [30] IDAE, Technical Conditions for PV Installations Connected to the Grid [in Spanish], Spanish Government Technical Report. Report Available from the Publication Services of the Institute for Diversification and Energy Savings, Spain, 2011. Available from: <http://www.idae.es>. (Accessed 6 June 2019).
- [31] S. Imahori, M. Yagiura, H. Nagamochi, Practical Algorithms for Two-Dimensional Packing, vol. 19, Department of Mathematical Informatics, University of Tokyo, 2006, p. METR2006.
- [32] A. Bortfeldt, A genetic algorithm for the two-dimensional strip packing problem with rectangular pieces, *Eur. J. Oper. Res.* 172 (2006) 814–837.
- [33] A. Lodi, S. Martello, D. Vigo, Recent advances on two-dimensional bin packing problems, *Discrete Appl. Math.* 123 (2002) 379–396.
- [34] A. Adamaszek, A. Wiese, A quasi-PTAS for the two-dimensional geometric knapsack problem, in: Proc. 26th ACM-SIAM Sympos. Discrete Algorithms, SIAM, 2015, pp. 1491–1505.
- [35] E.G. Birgin, R.D. Lobato, R. Morabito, An effective recursive partitioning approach for the packing of identical rectangles in a rectangle, *J. Oper. Res. Soc.* 61 (2010) 306–320.
- [36] V. Puroza, R. Morabito, Some experiments with a simple tabu search algorithm for the manufacturer's pallet loading problem, *Comput. Oper. Res.* 33 (2006) 804–819.
- [37] S.S. Mathur, T.C. Kandpal, B.S. Negi, Optical design and concentration characteristics of linear Fresnel reflector solar concentrators-I. Mirror elements of varying width, *Energy Convers. Manag.* 31 (1991) 205–219.
- [38] S.S. Mathur, T.C. Kandpal, B.S. Negi, Optical design and concentration characteristics of linear Fresnel reflector solar concentrators- II. Mirror elements of equal width, *Energy Convers. Manag.* 31 (3) (1991) 221–232.
- [39] J.A. Duffie, W.A. Beckman, *Solar Engineering of Thermal Processes*, fourth ed., John Wiley & Sons, New York, 2013.
- [40] M. Binotti, G. Manzolini, G. Zhu, An alternative methodology to treat solar radiation data for the optical efficiency estimate of different types of collectors, *Sol. Energy* 110 (2014) 807–817.
- [41] M.A. Moghimi, K.J. Craig, J.P. Meyer, A novel computational approach to combine the optical and thermal modelling of Linear Fresnel Collectors using the finite volume method, *Sol. Energy* 116 (2015) 407–427.
- [42] V.M. Sharma, J.K. Nayak, S.B. Kedare, Comparison of line focusing solar concentrator fields considering shading and blocking, *Sol. Energy* 122 (2015) 924–939.
- [43] P.H. Theunissen, W.A. Beckman, Solar transmittance characteristics of evacuated tubular collectors with diffuse back reflectors, *Sol. Energy* 35 (1985) 311–320.
- [44] M. Bruck, P. Sandborn, N. Goudarzi, A leveled cost of energy (LCOE) model for wind farms that include power purchase agreements (PPAs), *Renew. Energy* 122 (2018) 131–139.
- [45] IRENA. IRENA, *Renewable Energy Technologies: Cost Analysis Series, CSP*, 2012.
- [46] S. Abdelhady, D. Borello, A. Shaban, Techno-economic assessment of biomass power plant fed with rice straw: sensitivity and parametric analysis of the performance and the LCOE, *Renew. Energy* 115 (2018) 1026–1034.
- [47] S. Abdelhady, D. Borello, E. Tortora, Design of a small scale stand-alone solar

thermal co-generation plant for an isolated region in Egypt, Energy Convers. Manag. 88 (2014) 872–882.

- [48] T.T.D. Tran, A.D. Smith, Incorporating performance-based global sensitivity and uncertainty analysis into LCOE calculations for emerging renewable energy technologies, Appl. Energy 216 (2018) 157–171.
- [49] Andalusian Energy Agency (AEA). <https://www.agenciaandaluzadelaenergia.es/Radiacion/radiacion1.php>.
- [50] NREL. National, Renewable Energy Laboratory, Available on line at, 2019., <https://www.nrel.gov/docs/fy10osti/48662.pdf>.

Nomenclature of the Cost Analysis.

k^A : Assembly (€)
 k^{AT} : Absorber tube (€/kg)
 k^C : Controller (€)
 k^{CR} : Receiver cavity (€/m²)
 k^F : Foundation (€/m³)
 k^{GC} : Glass covering (€/m²)
 k^I : Insulation (€/m²)
 k^{MD} : Stepper motor and driver (€)
 k^{MIU} : Mirror unit (€/unit)
 k^{MoU} : Movement unit (€/unit)

k^{PC} : Protective casing (€/m²)
 k^R : Rail support (€/m)
 k^{St} : Structure (€/kg)
 k^{frame} : Frame (€/m²)
 k^{mirror} : Mirror (€/m²)
 $k^{pinion\ gear}$: Pinion gear (€/pinion gear)
 k^{Se} : Sensors (€)
 $k^{shaft\ Mi}$: Shaft mirror (€/m)
 $k^{shaft\ SRS}$: Secondary reflector system (€/m)
 L_{AT} : Absorber tube (m)
 L_{FS} : Fixed structure (m)
 L_{MS} : Mobile structure (m)
 L_M : Mmirrors (m)
 L_{SRS} : Secondary reflector system structure (m)
 L_a : Single absorber tube (m)
 L_{rail} : Rail support (m)
 L_{shaft} : Shaft of the a mirror (m)
 V_F : Foundation (m³)
 W_{AT} : Absorber tube (kg)
 W^U : Unitario (kg/m)
 W_{FS} : Fixed structure (kg)
 W_{MS} : Mobile structure (kg)
 W_{SRS} : Secondary reflector system structure (kg)